# Structural Characterization of the Apo Form of a Calcium Binding Protein from *Entamoeba histolytica* by Hydrogen Exchange and Its Folding to the Holo State

Sulakshana Mukherjee, Kavita Kuchroo, and Kandala V. R. Chary*

*Department of Chemical Sciences, Tata Institute of Fundamental Research, Homi Bhabha Road, Mumbai 400 005, India*

*Received April 15, 2005; Revised Manuscript Received June 28, 2005*

ABSTRACT: One of the calcium binding proteins from *Entamoeba histolytica* (*Eh*CaBP) is a 134 amino acid residue long ($M_r$ ~14.9 kDa) double domain EF-hand protein containing four $Ca^{2+}$ binding sites. CD and NMR studies reveal that the $Ca^{2+}$-free form (apo-*Eh*CaBP*)* exists in a partially collapsed form compared to the $Ca^{2+}$-bound (holo) form, which has an ordered structure (PDB ID 1JFK). Deuterium exchange studies on the partially structured apo-*Eh*CaBP reveal that the C-terminal domain is better structured than the N-terminal domain. The protein can be reversibly folded and unfolded upon addition of $Ca^{2+}$ and EGTA, respectively. Titration shows a slow initial folding of the apo form with increasing $Ca^{2+}$ concentration, followed by a highly cooperative folding to its final state at a certain threshold of $Ca^{2+}$. $Ca^{2+}$ and the EGTA titration taken together show that site II in the N-terminal domain has the highest affinity for $Ca^{2+}$ contrary to earlier studies. Further, this study has thrown light on the relative $Ca^{2+}$ binding affinity and specificity of each site in the intact protein. A structural model for the partially collapsed form of apo-*Eh*CaBP and its equilibrium folding to its completely folded holo state has been suggested. Large conformational changes seen in transforming from the apo to holo form of *Eh*CaBP suggest that this protein should be functioning as a sensor protein and might have a significant role in host−parasite recognition.

EF-hand $Ca^{2+}$ binding proteins (hereafter referred to as EF-CaBP) belong to a growing superfamily of $Ca^{2+}$ binding proteins. Ever since the recognition of the EF-hand motif in the parvalbumin structure in 1973 (*1*), more than 1000 distinct primary sequences in this class of proteins are known (*2*, *3*). They bind cooperatively to $Ca^{2+}$ in the subnanomolar to millimolar range and function as signal transducers or modulators. Some of them have been found to be involved in extracellular functions such as cell migration, differentiation, and association (*4*). These proteins have been a subject of great interest for structural biologists, resulting in the availability of more than 300 three-dimensional (3D) structures, as of today (*2*, *3*, *5*), both by NMR[1] spectroscopy and by X-ray crystallography. Interestingly, most of the known 3D structures of $Ca^{2+}$-free (apo form) EF-CaBPs are revealed by high-resolution NMR spectroscopy. Besides studying the 3D structures and dynamics of these proteins, there have been several attempts to understand the $Ca^{2+}$ affinity, cooperativity, selectivity, and displacement among the various EF-hand units present in a given protein (*2*, *3*, *6*−*8*).

Calmodulin- (CaM-) like $Ca^{2+}$-dependent regulatory proteins undergo major conformational change upon $Ca^{2+}$ binding (*2*, *3*, *9*−*12*), exposing hydrophobic moieties to interact with target proteins. In contrast, calbindin $D_{9K}$-like $Ca^{2+}$-buffer/transport proteins (*2*, *3*) do not undergo any conformational change upon $Ca^{2+}$ binding and hence do not expose any hydrophobic moieties in either their apo or holo forms. Yet another variant of EF-CaBPs is found to lose a significant amount of tertiary structure in its apo form (*13*−*17*), which it regains after $Ca^{2+}$ binding. Recently, a number of EF-CaBPs have been reported to have molten globular characteristics in their apo form (*13*−*17*). The structural characterization of this class of proteins in their apo form becomes very challenging, either by X-ray or by NMR, owing to their flexibility. They form poor or no crystals for X-ray study and show narrow dispersion in backbone $^1H^N$ chemical shifts coupled with large line broadening for NMR study. The study involving such partially collapsed structures and their equilibrium folding to its native holo states provides an insight into the protein folding and as well as signal transduction mechanisms of EF-CaBPs, which might be different from the well-established mechanisms of CaM, troponin C (TnC), recoverin, and so on, which have well-folded apo as well as holo structures (*18*−*20*).

An EF-hand $Ca^{2+}$ binding protein from *Entamoeba histolytica* (an intestinal parasite and a causative agent of amoebiasis and amoebic dysentery, which is a significant source of morbidity and mortality in developing countries) is a 134 amino acid residue long ($M_r$ ~14.9 kDa) monomeric protein containing four canonical EF-hand $Ca^{2+}$ binding loops (*21*). Calcium is thought to be involved in the pathogenetic mechanisms of amoebiasis (*22*), and the mechanisms governing pathogenesis are yet not clear. To understand the mechanisms by which calcium affects virulence, a gene encoding a novel calcium binding protein from *E.*

* To whom correspondence should be addressed. E-mail: chary@tifr.res.in. Phone: 91-22-2278 2489. Fax: 91-22-2280 4610.

[1] Abbreviations: NMR, nuclear magnetic resonance; ITC, isothermal calorimetry; HSQC, heteronuclear single-quantum coherence; *Eh*CaBP, *Entamoeba histolytica* calcium binding protein; CaM, calmodulin; TnC, troponin C; EGTA, ethylene glycol bis(*β*-aminoethyl ether)-*N*,*N*,*N*′,*N*′-tetraacetate.

10.1021/bi050691h CCC: $30.25 
Published on Web 08/04/2005

*histolytica* (hereafter referred as *Eh*CaBP) was isolated. A high-resolution 3D solution structure of the protein thus expressed has been determined in its holo form (PDB ID 1JFK) (*5*). *Eh*CaBP shares about 29% sequence identity with the well-studied EF-hand protein CaM (*5*, *23*). Similarity in the protein sequence of *Eh*CaBP and CaM is restricted to EF-hand $Ca^{2+}$ binding loops with a significant dissimilarity in the functional central linker region. The structural topology of *Eh*CaBP resembles that of CaM and TnC with two globular domains (the N- and C-terminals) connected by a flexible eight amino acid residue linker.

The apo form of *Eh*CaBP (hereafter referred to as apo-*Eh*CaBP) is highly dynamic, yielding broad NMR lines and poor $^1H^N$ chemical shift dispersion. Despite these hindrances, a structural model has been developed for the apo-*Eh*CaBP and its equilibrium folding to the completely folded holo state. This study also throws light upon the relative $Ca^{2+}$ binding affinities and specificities among the four metal binding sites.

## EXPERIMENTAL PROCEDURES

*Protein Expression and Purification.* The protocol described earlier (*5*, *23*) was used for overexpression of *Eh*CaBP in minimal (M9) medium. The purification protocol was the same as described earlier except for the fact that, instead of 10 mM $CaCl_2$, 100 mM NaCl was used for elution from the DE-52 column with a flow rate of 0.25 mL/min. Presence of protein in each of the eluted fractions (2 mL) was monitored by the absorbance at 280 nm and checked on SDS−PAGE. The protein fractions thus obtained were concentrated to 1 mL in an Amicon ultrafiltration cell using 3 kDa cutoff membranes. The concentrate was then loaded in a 1 cm × 150 cm Sephadex G-50 column, preequilibrated with Tris−EGTA buffer (50 mM Tris, 0.5 mM EGTA, pH 6.5). The eluted fractions were once again screened for the apo protein by absorbance at 280 nm. All labeled chemicals used were either from Cambridge Isotopes Ltd. or from Spectra Stable Isotopes (Spectra Gases Inc). Other chemicals required were of ultrapure grade from Sigma-Aldrich and SRL. The purity and yield of the protein in the eluted fractions were confirmed by SDS−PAGE (15%) and matrix-assisted laser desorption /ionization time-of-flight (MALDI-TOF) mass spectroscopy. The fractions were collected and concentrated by ultrafiltration for NMR and other biophysical studies. Experiments reported here have been conducted at 25 °C in the presence of 100 mM NaCl. Plastic ware and Chelex-100-treated buffers were used throughout to avoid $Ca^{2+}$ contamination. The ANS binding was used as a measure to check any $Ca^{2+}$ contamination in the protein free of EGTA and after deliberate addition of EGTA since a slightest presence of $Ca^{2+}$ causes a drastic change in the fluorescence signal.

*Dynamic Light Scattering.* The hydrodynamic radius ($R_h$) of individual molecules of the apo form of *Eh*CaBP to ascertain its state of oligomerization was measured using the *d*ynamic *l*ight *s*cattering (DLS; Dynapro-LS instrument of Protein Solutions) method. The software "Regularization", provided by Protein Solutions, was used in analyzing the results. Standard synthetic beads of 6.0 nm diameter (provided by Protein Solutions) and solutions of bovine serum albumin (3.0 nm) were used as standards. Measurements were made at protein concentrations used in NMR experiments (850 $\mu$M).

Table 1: Elution Characteristics of *Eh*CaBP in $Ca^{2+}$-Free and $Ca^{2+}$-Bound Forms

| *Eh*CaBP | $K_{av}$[a] | apparent relative molecular mass[b] |
|---|---|---|
| $Ca^{2+}$-free form (apo) | 0.400 | 21.67 ± 0.03 |
| $Ca^{2+}$-bound form (holo) | 0.451 | 16.8 ± 0.03 |

[a] $K_{av} = (V_x - V_0)/(V_t - V_0)$, where $V_0$ is the void volume, $V_t$ the total volume of the gel bed, and $V_x$ the elution volume of the protein. [b] Based on the molecular mass markers (see text).

*Circular Dichroism.* CD spectra were recorded on JASCO J-810 spectropolarimeter equipped with a peltier-controlled temperature controller and 0.1 and 1 cm path length cuvettes for recording far- and near-UV spectra, respectively. Far- and near-UV spectra were recorded in 0.5 nm steps from 250 to 200 nm and from 300 to 260 nm, respectively, with an integration time of 2 s at each wavelength and baseline corrected against a cuvette containing buffer alone. Thermal stability was determined by monitoring the molar ellipticity at 222 nm as a function of temperature at 2 °C intervals with 3 min equilibration and a collection time of 30 s at each temperature. At the end of each thermal unfolding experiment, the sample was cooled immediately to 20 °C, and spectra were recorded to obtain the extent of refolding. Protein solutions of 31 and 75 $\mu$M were used for far- and near-UV CD, respectively. The CD data thus obtained, in millidegrees, were expressed in terms of mean residue ellipticity [$\Theta$], in deg·cm$^2$·dmol$^{-1}$.

*Gel Permeation.* Protein samples (300 $\mu$L of 39 $\mu$M) in 50 mM Tris-HCl buffer and 100 mM NaCl, pH 7.4, in the presence of 0.5 mM EGTA (apo) or/and 10 mM $Ca^{2+}$, were applied on a Superdex G-75 gel permeation column (120 mL bed volume), equilibrated in the same buffer, and connected to the low-pressure liquid chromatography system (Bio-Rad). The elution characteristics, together with the apparent molecular masses, estimated using ribonuclease A, ovalbumin, BSA, and alcohol dehydrogenase as molecular markers, are shown in Table 1. Each measurement was carried out at least three times for reproducibility. The void volume was determined using Blue dextran.

*ANS Binding.* ANS binding experiments were performed on a spectrofluorometer (SPEX Fluorolog) at 25 °C with excitation and emission slits of 0.7 nm using 1 mL of 10.35 $\mu$M apo-*Eh*CaBP in 50 mM Tris-HCl and 100 mM NaCl. To monitor the changes in ANS fluorescence emission spectra, 1 mL of 10.35 $\mu$M apo and holo forms was taken in 50 mM Tris-HCl and 100 mM NaCl. ANS fluorescence emission spectra were recorded between 400 and 600 nm with excitation at 389 nm. The protein was saturated with 115 $\mu$M ANS. The spectra were corrected for ANS fluorescence in buffer without the protein.

*NMR.* NMR experiments were carried out on a Varian INOVA 600 MHz NMR spectrometer equipped with a pulsed field gradient unit and triple resonance probe with an actively shielded *Z*-gradient, operating at a $^1H$ frequency of 599.862 MHz. Sensitivity-enhanced 2D [$^{15}N-^1H$] heteronuclear single-quantum correlation (HSQC) (*24*) spectra of the protein sample (pH 6.5 and temperature = 25 °C) were recorded with the $^1H$ carrier placed on the $H_2O$ resonance

(4.78 ppm) and the $^{15}N$ carrier at 123.8 ppm. During the course of all experiments, the protein samples were found to be stable and did not change or degrade with time. $^{1}H$ chemical shifts were calibrated relative to 2,2-dimethyl-2-silapentane-5-sulfonate (DSS) at 288 K (0.0 ppm); $^{15}N$ chemical shifts were calibrated with respect to an external standard of $^{15}NH_4Cl$ (2.9 M in 1 M HCl). Spectra were processed using VNMR 6.1B (Varian) and Felix 2002 (Molecular Simulations Inc.). The 2D [$^{15}N-^{1}H$]-HSQC spectra were typically apodized using a 90°-shifted sine square bell window function along both dimensions before zero-filling and 2D Fourier transformation. Integral volumes (in arbitrary units) for the individual $^{15}N-^{1}H$ cross-peaks in these spectra were measured using Felix.

*Hydrogen Exchange of Backbone Amide Protons in the Apo-EhCaBP.* Approximately 110 mg of the apo form of uniformly $^{15}N$-labeled *Eh*CaBP was taken in 50 mM Tris-HCl buffer (pH = 6.5) to prepare 15 identical samples, each 580 $\mu$L with identical protein concentration (0.95 mM). Samples were lyophilized and redissolved in 550 $\mu$L of ice-cold $^{2}H_2O$, one after another. This was done primarily to allow amide protons to exchange with $^{2}H$ during a time, ranging from 0 to 1000 s. Immediately after such varying delay time interval (0, 10, 45, 60, 100, 125, 150, 300, 450, 720, and 1000 s) for HX exchange, 30 $\mu$L of ice-cold 1 M $CaCl_2$ solution taken in $^{2}H_2O$ was added to transform the protein into its holo form and followed immediately by recording a 2D [$^{15}N-^{1}H$]-HSQC spectrum. The addition of $Ca^{2+}$ quenches the HX exchange reaction of amide protons, used as probes in the characterization of the apo state of *Eh*CaBP. One of the samples prepared in a mixed solvent of 90% $H_2O$ plus 10% $^{2}H_2O$ was used to shim the magnet and tune and match the radiofrequency coil prior to the above series of experiments. For checking reproducibility, 0, 100, and 450 s interval experiments were repeated twice. For the 0 s time interval experiments, 580 $\mu$L of 50 mM ice-cold $CaCl_2$ solution in $^{2}H_2O$ was directly added to the lyophilized protein to record the 2D [$^{15}N-^{1}H$]-HSQC spectrum. The corresponding data were used for having a qualitative insight and were ignored in all quantifications.

*HX Exchange Rates.* The HX exchange rates of individual backbone amide protons in *Eh*CaBP in the apo state were measured indirectly by monitoring the amide proton decays by measuring the integral volumes of the nonoverlapping peaks. Each datum was normalized with respect to the averaged peak volume of V97, which did not vary during the time range under investigation. The decay of the individual peak volumes was fitted to the single exponential decay. The protection factors (PF) were measured as PF = $k_{ch}/k_{ex}$, where $k_{ch}$ and $k_{ex}$ are the calculated intrinsic exchange and experimental exchange rates, respectively (*25*).

*$Ca^{2+}$ Titration of EhCaBP.* $Ca^{2+}$ titration was carried out with 100 mM $CaCl_2$ whose concentration was estimated by AAS with a precision of 2%. The protein concentration was 1 mM in 50 mM Tris-HCl (pH = 6.5) and 100 mM NaCl. For each titration, an aliquot of 1 $\mu$L of the stock solution was added to the NMR tube containing the protein solution and mixed, followed by recording 2D [$^{15}N-^{1}H$]-HSQC spectra at 25 °C. The total experimental time for each 2D HSQC was 20 min, and the total volume added was 30 $\mu$L. During the entire course of the titration no transient aggregation was observed as monitored by DLS experiments for each step, and the sample was found to be soluble and stable. At the end of the titration, the change in pH was less than 0.1. HSQC spectra were processed with identical processing parameters.

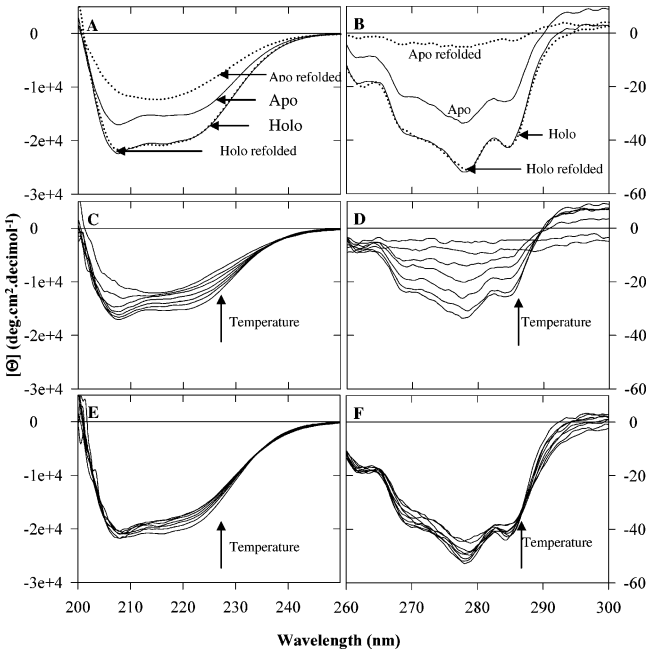


FIGURE 1: (A) Far-UV and (B) near-UV CD spectra of apo- and holo-*Eh*CaBP at 20 °C before and after heating to 95 °C. Temperature dependence of far-UV CD spectra of apo-*Eh*CaBP (C) and holo-*Eh*CaBP (E). Temperature dependence of near-UV CD spectra of apo-*Eh*CaBP (D) and holo-*Eh*CaBP (F).

*Ethylene Glycol Bis(β-aminoethyl ether)-N,N,N′,N′-tetra-acetate (EGTA) Titration of Holo-EhCaBP As Monitored by NMR.* EGTA titration was carried out with 100 mM EGTA. The protein concentration was ~0.77 mM in 50 mM Tris-HCl (pH = 6.5) and 100 mM NaCl. For each titration, an aliquot of 2.0 $\mu$L of the stock solution was added to the NMR tube containing the protein solution and mixed thoroughly, followed by recording 2D [$^{15}N-^{1}H$]-HSQC spectra at 25 °C. The total experimental time for each 2D-HSQC was 20 min. The total volume added was 50 $\mu$L.

## RESULTS

*Apo-EhCaBP.* Unlike the holo form of the protein, which is highly thermostable, apo-*Eh*CaBP is unstable at higher temperatures (>25 °C). Hence, experiments discussed here in this paper were carried out at 25 °C in the presence of 100 mM NaCl concentration.

Dynamic light scattering (DLS; Dynapro-LS instrument of Protein Solutions) and matrix-assisted laser desorption/ionization time-of-flight (MALDI-TOF) mass spectroscopy results reveal the monomeric nature and the purity of the sample, respectively. The gel permeation experimental results (see Table 1) reveal that the apparent relative molecular masses for holo- and apo-*Eh*CaBP as 16.8 and 21.7 kDa, respectively. The theoretical relative molecular mass for holo-*Eh*CaBP is 14.9 kDa.

Panels A and B of Figure 1 show the far- and near-UV regions of the CD spectra of both apo and holo forms of *Eh*CaBP, respectively. As is evident in Figure 1A, the bands around 208 and 222 nm, which are largely due to exciton splitting of the $\pi-\pi^*$ absorption band and a $n-\pi^*$ transition,

respectively, are representative of predominantly α-helical conformation, which partially collapse in transforming from the holo to apo form. On the other hand, though *Eh*CaBP is devoid of Trp residues, it is rich in Tyr (four residues) and Phe (nine residues) residues, and the bands for the corresponding residues are well resolved in the near-UV CD. The CD shows two negative broad bands at 278 and 285 nm (6 nm red-shifted band) for Tyr. The vibronic bands arising from Phe residues are well resolved with minima at 262 and 268 nm. Large changes seen in this part of the CD spectrum (Figure 1B), in going from the holo to apo form of *Eh*CaBP, support partial collapse of the tertiary structure of *Eh*CaBP.

*Temperature Dependence of Far-UV CD Spectra.* In holo-*Eh*CaBP, the effects of temperature, in going from 20 to 95 °C, are marginal around both 208 and 222 nm (Figure 1E). The values of both $\theta_{208}$ and $\theta_{222}$ reversibly change from $-2.2 \times 10^4$ to $-2.1 \times 10^4$ and from $-1.9 \times 10^4$ to $-1.7 \times 10^4$ deg·cm$^2$·dmol$^{-1}$, respectively. In apo-*Eh*CaBP, the temperature effects in the negative values of ellipticity are more prominent in going from 20 to 95 °C (Figure 1C), and the values of $\theta_{208}$ and $\theta_{222}$ irreversibly change from $-1.7 \times 10^4$ to $-1.1 \times 10^4$ and from $-1.5 \times 10^4$ to $-1.0 \times 10^4$ deg·cm$^2$·dmol$^{-1}$, respectively. Thermal unfolding experiments reveal that the extent of refolding in the case of holo-*Eh*CaBP is 100%, while in the case of apo-*Eh*CaBP, the secondary structure signature seen before heating cannot be retrieved (Figure 1A). These results reiterate that holo-*Eh*CaBP is thermally stable, while the apo-*Eh*CaBP is sensitive to even small changes in temperature. It also reveals that there is a substantial collapse in the secondary structure in transforming from its holo to apo form (Figure 1A).

*Temperature Dependence of Near-UV CD Spectra.* The temparture dependence of near-UV CD spectra of both forms of *Eh*CaBP are shown in Figure 1D,F. In holo-*Eh*CaBP, the effects of temperature, in going from 25 to 95 °C, are minimal at and around the vibronic bands of tyrosine and phenylalanine. They change reversibly by a small amount (Figure 1F). On the other hand, for apo-*Eh*CaBP, the temperature effects in the negative values of ellipticity are more prominent in going from 20 to 95 °C, around the Tyr and Phe bands (Figure 1D). The changes in them are found to be irreversibly large (Figure 1B,F). As in the case of the far-UV CD spectra, thermal unfolding experiments reveal that the extent of refolding in the case of holo-*Eh*CaBP is complete, while in the case of apo-*Eh*CaBP, the secondary structure signature seen before heating cannot be retrieved (Figure 1B). These results once again reiterate that holo-*Eh*CaBP is thermally stable, while the apo-*Eh*CaBP is sensitive to even small changes in temperature. There is a partial collapse of tertiary structure of *Eh*CaBP in transforming from its holo to apo form (Figure 1B).

*Interaction with 8-Anilino-1-naphthalenesulfonic Acid (ANS).* ANS fluorescence is strongly dependent on the local environment. As shown in Figure 2, the emission is weak in water with a maximum at 515 nm. ANS binds to both apo- and holo-*Eh*CaBP, resulting in significant enhancement in the fluorescence associated with large blue shifts, 39 and 43 nm, respectively. The fluorescence intensity is higher for the holo form compared to apo-*Eh*CaBP. The enhancement in the fluorescence is 3- and 11-fold, in the case of apo- and holo-*Eh*CaBP, respectively, as compared to completely unfolded *Eh*CaBP (denatured by 8 M Gdn·HCl). These data

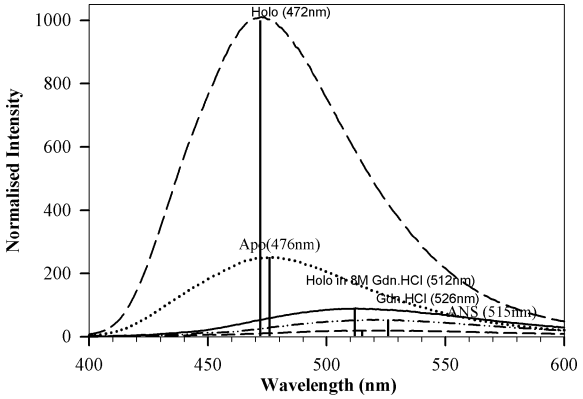


FIGURE 2: ANS binding to apo, holo, and unfolded (holo in 8 M Gdn·HCl) forms of *Eh*CaBP.

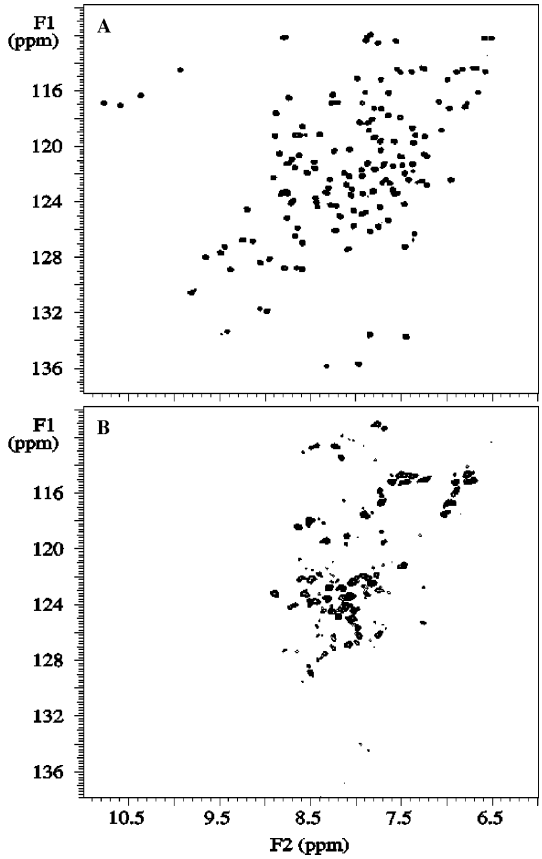


FIGURE 3: 2D [$^{15}$N-$^{1}$H]-HSQC spectra of (A) holo-*Eh*CaBP and (B) apo-*Eh*CaBP.

suggest that apo-*Eh*CaBP exhibits substantial hydrophobic pockets, which are, however, smaller compared to those in holo-*Eh*CaBP.

*2D [$^{15}$N−$^{1}$H]-HSQC Spectrum of Apo-EhCaBP.* Panels A and B of Figure 3 show [$^{15}$N−$^{1}$H]-HSQC spectra of the holo- and apo-*Eh*CaBP, respectively. The spectrum of apo-*Eh*CaBP (Figure 3B), with a narrow dispersion in backbone $^{1}H^{N}$ chemical shifts (7.20−8.75 ppm), accounts for only one-third of the expected peaks, suggesting that most of the peaks are broad (*26*, *27*) due to constrained conformational fluctuations on the micro- and millisecond time scale (*28*, *29*). Addition of 10 mM $CaCl_2$ transforms the protein into the holo form, and the [$^{15}$N−$^{1}$H]-HSQC spectrum (Figure 3A) thus recorded is identical to the previously recorded spectrum of the holoprotein.

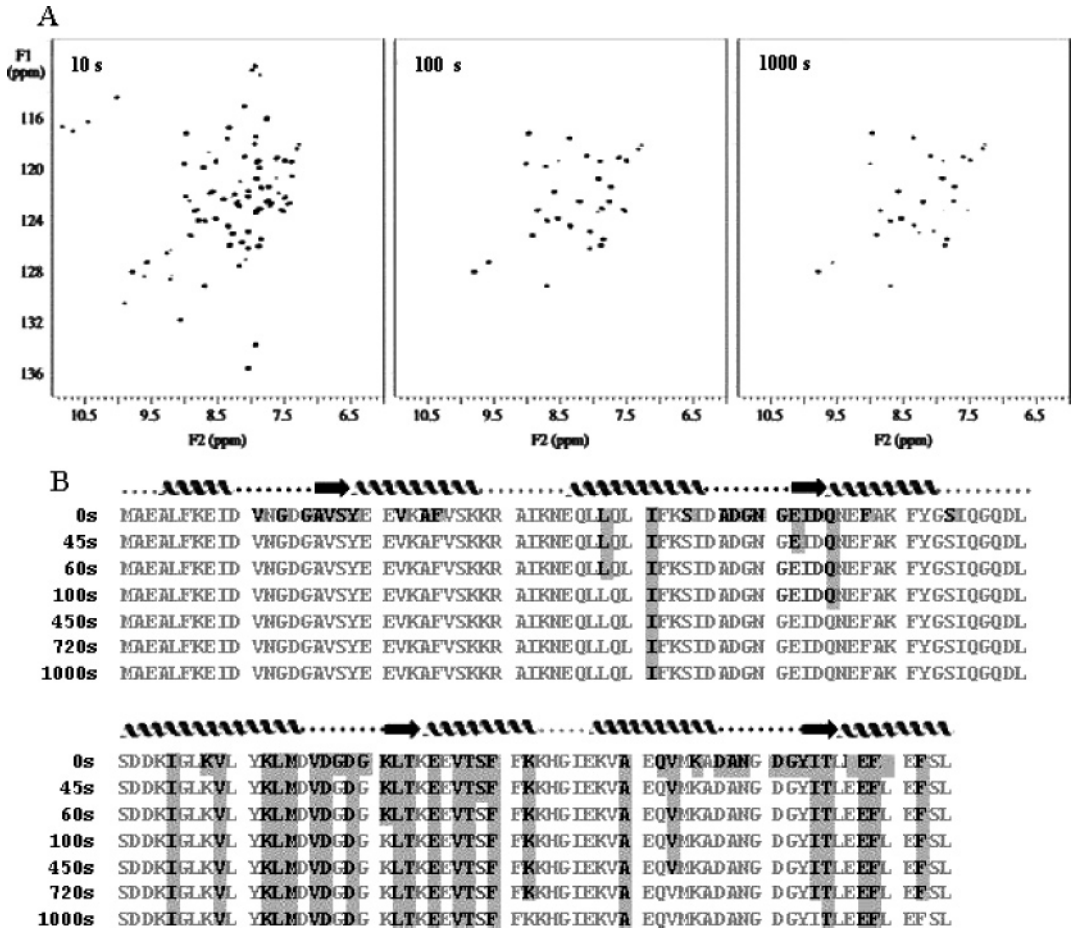


FIGURE 4: (A) 2D [$^{15}N-^{1}H$]-HSQC spectrum of *Eh*CaBP immediately after the addition of $^{2}H_2O$ and $Ca^{2+}$ to the apo-*Eh*CaBP, with an interval of 0, 100, and 1000 s between the two additions. For details see Experimental Procedures. (B) Qualitative analysis of the $^{2}H_2O$ exchange experimental data of the apo-*Eh*CaBP. The amino acid residues with intact $^{1}H^{N}$ are shown in black with a gray background, and those which exchange fast are shown in gray. The secondary structural elements are shown above the primary sequence of the protein.

*Hydrogen Exchange of Backbone Amide Protons in Apo-EhCaBP.* As evident from Figure 3B, it is difficult to get any insight on the conformation of apo-*Eh*CaBP. We could not assign the spectrum as it suffers from extensive spectral overlap. This hints at the collapse of secondary and tertiary structures and supports observations made from CD data described above. A deuterium exchange study shows that all of the [$^{15}N-^{1}H$] peaks disappear within 15 min at 25 °C, substantiating our conclusion that the apo form has a collapsed tertiary structure. The [$^{1}H-^{2}H$] exchange of backbone amide protons in apo-*EhCaBP* has been monitored indirectly by transforming it into its holo form with the sudden addition of a $Ca^{2+}$ pulse, as described in Experimental Procedures. As illustrative examples, Figure 4A shows the [$^{15}N-^{1}H$]-HSQC spectra recorded with 0, 100, and 1000 s time interval between the $^{2}H_2O$ pulse and the $Ca^{2+}$ pulse. From the 0 s time interval spectrum (Figure 4A) one can infer about the intact nature of around 60 amide protons, which are assigned from the previous knowledge of shifts in the holo state (see Figure 4B). To quantify the [$^{1}H-^{2}H$] exchange rates ($k_{ex}$) of individual backbone amide protons in apo-*Eh*CaBP, we monitored individual $^{1}H^{N}$ decays (see Figure 5A), and the corresponding protection factors (PF) have been measured. The $^{1}H^{N}$ PFs are given in Figure 5B. For comparison, PFs for most of the $^{1}H^{N}$ spins in the holo state were also measured as described in Experimental Procedures (see Figure 5B) (*30*, *31*). As evident from Figure 5B, PFs in the apo state are much smaller compared to the holo state. Relatively higher PFs are observed for the amide protons in the C-terminal domain compared to the N-terminal domain, suggesting a greater structural stability for the C-terminal domain. Within the C-terminal domain, the $^{1}H^{N}$ belonging to K91, L92, T93, I124, and T125 are highly protected. These residues incidentally belong to the two antiparallel $\beta$-strands in the holo state, indicating that the native (holo state) $\beta$-strands belonging to the C-terminal domain are intact. Further, most of the amide protons belonging to the E- and F-helices of the third EF-hand and the F-helix of the fourth EF-hand have higher PFs and hence higher structural stability. Interestingly, several residues belonging to the loop region of the third EF-hand are highly protected, indicating that this part has more stable structural elements compared to the fourth EF-hand. With regard to the overall conformation of the protein, the third EF-hand is the most protected one and hence may be relatively more structured. One of the reasons for this could be that the E-helix of this EF-hand is the longest of all eight helices seen in the holo state of the protein and contains more hydrophobic residues.

For the N-terminal domain, the data show more collapsed secondary and tertiary structural elements. From the 0 s time interval spectrum described above, we could infer about the intact nature of only 23 backbone amide protons in this domain. Unlike in the case of the C-terminal domain, only

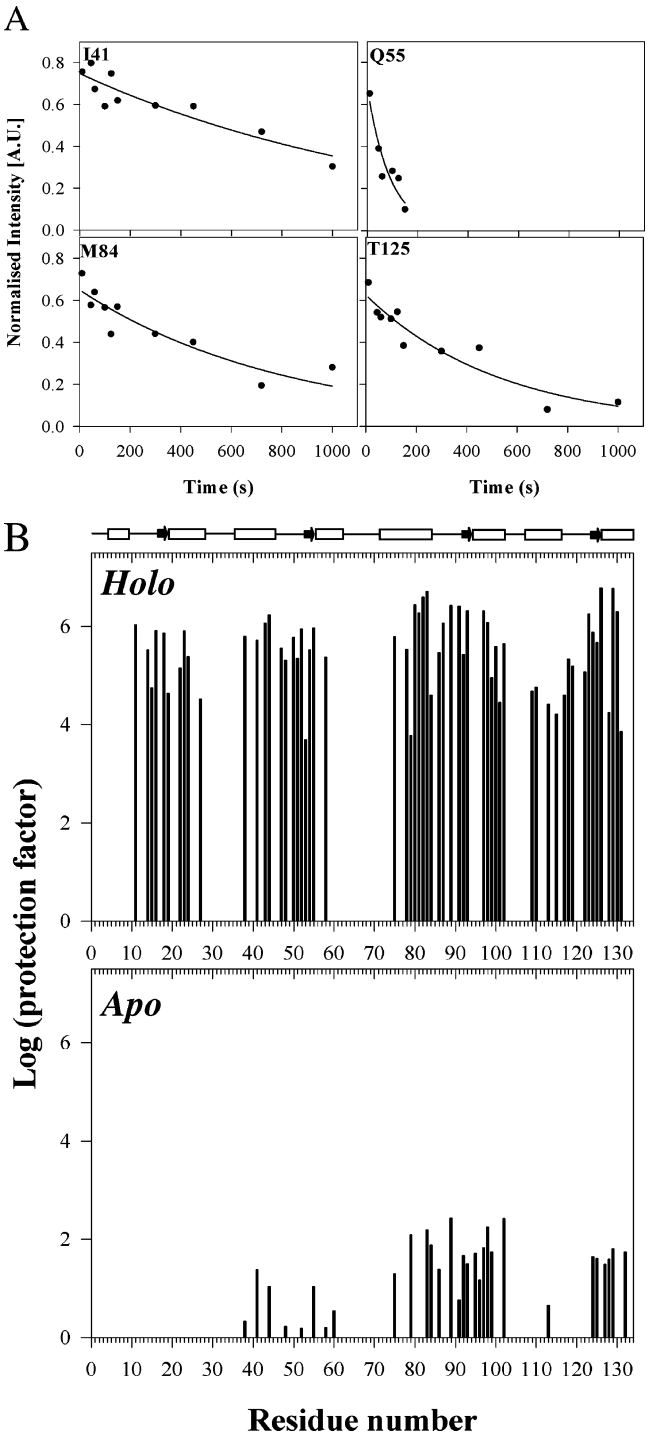


FIGURE 5: (A) Observed $^1H-^2H$ exchange kinetics for I41, Q55, M84, and T125. The $^1H^N$ occupancy was determined from the corresponding peak integral volumes measured in individual 2D [$^{15}N-^1H$]-HSQC spectra. Solid lines are the fitting curves. (B) Histograms showing the distribution of protection factors (PFs) from amide hydrogen exchange for holo- and apo-*Eh*CaBP. The PFs are plotted on a logarithmic scale. The secondary structural elements are shown schematically above the plots.

4 of them were seen in the next (45 s) time interval, indicating the weak structural stability of this domain. The amide proton belonging to I41 in the E-helix of the second EF-hand is found to be the most stable ($k_{ex} = 7.44 \times 10^4$ $s^{-1}$) in the entire N-terminal domain, followed by Q55 and L38 belonging to the F- and E-helices, respectively, of the second EF-hand.

Scheme 1

1 6 8 12

MAEALFKEI**DVNGD<u>G</u>A<u>V</u>SYEE**VKAFVSKKRAIKNEQ

LLQLIFKSI**DADGN<u>G</u>E<u>I</u>DQNE**FAKFYGSIQGQDLSDDKI

GLKVLYKLM**DVDGD<u>G</u>K<u>L</u>TKEE**VTSFFKKHGIE

KVAEQVMKA**DANGD<u>G</u>Y<u>I</u>TLEE**FLEFSL

*$Ca^{2+}$ Titration of Apo-EhCaBP.* During the course of $Ca^{2+}$ titration, several new signals started appearing in the HSQC spectrum, with the concomitant decrease of original peaks corresponding to the apo-*Eh*CaBP. The amide ($^1H^N$) protons of the Gly-6 (glycine at the sixth position) residues and the residues at the 8th position (Val/Ile/Leu) of all four $Ca^{2+}$ binding loops (shown with an underline in Scheme 1) exhibit characteristic downfield shifts in the $Ca^{2+}$-bound state of the protein. In the holo form, the amide ($^1H^N$) protons of Gly-6 are involved in hydrogen bonding with the side-chain carboxyl oxygen atom (C′O) of an invariant Asp at the first position of the respective $Ca^{2+}$ binding loops. On the other hand, the individual amide ($^1H^N$) protons of the residue at the eighth position of the $Ca^{2+}$ binding loops are in close vicinity of the carbonyl group (C′O) belonging to its N-terminal residue, which is the only backbone carbonyl oxygen that directly coordinates to $Ca^{2+}$ (*32*, *33*).

In the holo-*Eh*CaBP, the Gly-6 residues, G15, G51, G90, and G122, have their $^1H^N$ chemical shifts at 10.36, 10.78, 10.60, and 9.92 ppm, respectively, and show up in the least crowded region of the HSQC spectrum. Similarly, residues V17, I53, L92, and I124, with their $^1H^N$ chemical shifts at 9.51, 9.79, 8.89, and 9.68 ppm, respectively, also appear in a fairly resolved region. Thus, the residues at positions 6 and 8 constitute good markers to monitor the $Ca^{2+}$ binding process and also the protein folding. In the following, the four $Ca^{2+}$ binding sites present in *Eh*CaBP are identified as follows: (i) site I (residues 1−32), (ii) site II (residues 33−62), (iii) site III (residues 71−103), and (iv) site IV (residues 104−134).

*$Ca^{2+}$ Titration Up to a $Ca^{2+}$:EhCaBP(M/P) Ratio of 1:1.* During the initial stages of titration, there is gradual appearance of cross-peaks belonging to site II. As an illustration, Figure 6 shows selected regions of the HSQC spectrum. Figure 7 shows the volumes of cross-peaks as a function of the metal/protein ratio, plotted for residues at positions 6 (G15, G51, G90, and G122), 8 (V17, I53, L92, and I124), and 9 (S18, D54, T93, and T125) in all four metal binding sites of *Eh*CaBP, normalized with respect to the [$^{15}N-^1H$]-HSQC spectrum of $[Ca^{2+}]_4$-*Eh*CaBP. These plots indicate the percentage of various intermediate species present at different ratios of the metal and the protein. The primary observation revealed at this stage of titration is that the $Ca^{2+}$ binds first to the N-terminal domain and specifically to site II.

*$Ca^{2+}$ Titration beyond a $Ca^{2+}$:EhCaBP Ratio of 1:1.* At a M/P ratio of 1:1, with site II partially filled with $Ca^{2+}$, the added $Ca^{2+}$ continues to bind to site II up to a metal/protein ratio of 2:1. Beyond this, it starts binding to sites I, III, and IV, as shown in Figure 7. During this stage of titration (M/P ratio of 2−3), two important observations are made: (i) there is almost simultaneous appearance of peaks corresponding

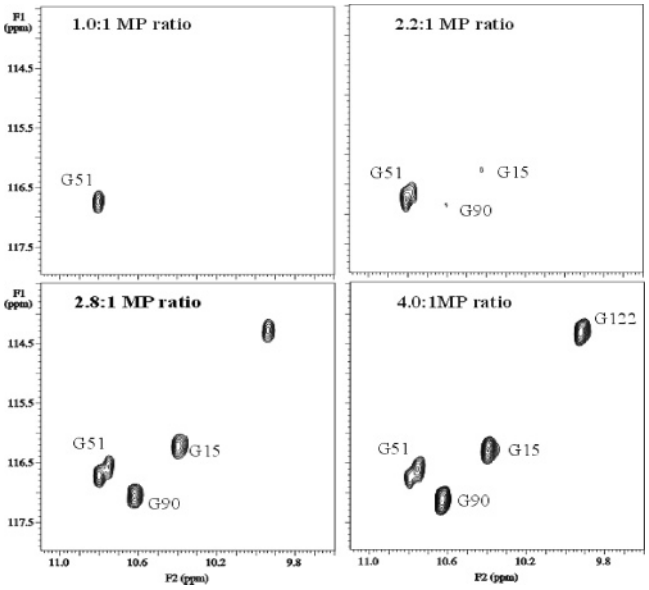


FIGURE 6: Selected region of 2D [$^{15}$N−$^{1}$H]-HSQC spectra recorded during the $Ca^{2+}$ titration of *Eh*CaBP showing G15, G51, G90, and G122 peaks at different M/P ratios. The M/P ratio is indicated at the top left of all four panels.

to the remaining sites (I, III, and IV) and (ii) the rate of growth of the corresponding peaks with respect to the $Ca^{2+}$ concentration suddenly increases around a M/P ratio of 2.5 and saturates at a metal/protein ratio of 4 (Figure 7). Beyond the M/P ratio of 1:4, no changes were seen in the [$^{15}$N−$^{1}$H]-HSQC spectrum.

*EGTA Titration of Holo-EhCaBP*. To study the reversibility of the folding pathway, EGTA titration of holo-*Eh*CaBP was carried out by monitoring changes in the HSQC spectrum. As in the case of the $Ca^{2+}$ titration, once again Gly-6 were used as markers. During titration, new signals started appearing in the HSQC spectrum, with the concomitant decrease of the original peaks corresponding to the holo form. Figure 8 shows the normalized volumes of cross-peaks plotted for the four Gly-6 residues chosen as markers. These plots indicate the percentage of various intermediate species present at different ratios of the metal and the protein. An important observation during EGTA titration is that the folding pathway observed during the $Ca^{2+}$ titration of *Eh*CaBP is reversible. As evident from Figure 8, EGTA first dislodges $Ca^{2+}$ from site IV, followed by sites I and III. Finally, $Ca^{2+}$ is slowly chelated from site II.

## DISCUSSION

*Structural Characterization of Apo-EhCaBP*. Size-exclusion chromatography results reveal that apo-*Eh*CaBP is predominantly in a monomeric form and rule out any kind of protein aggregation. The DLS data (data not shown) also rule out any possibility of higher aggregates even at NMR concentrations of the protein. Gel permeation experimental results (see Table 1) suggest that, in contrast with the $Ca^{2+}$-bound form, the apoprotein has significantly expanded globular volume. Apo-*Eh*CaBP is unstable and sensitive to temperature, unlike holo-*Eh*CaBP. Besides, all $^{1}H^{N}$ in apo-*Eh*CaBP are found to exchange very fast upon the addition of $^{2}H_2O$. In contrast to those in holo-*Eh*CaBP, the $^{1}H^{N}$−$^{2}H^{N}$ exchange rates in apo-*Eh*CaBP, which were monitored indirectly by transforming it into its holo form, are also very fast. All of these observations taken together indicate that the apo form has a collapsed tertiary structure or molten globule-like structure. This is also reflected in the CD spectra, which showed significant collapse of secondary and tertiary structures seen in the holo form. Upon addition of $Ca^{2+}$, the molten globular structure completely gets transformed into its native 3D structure seen in its holo state.

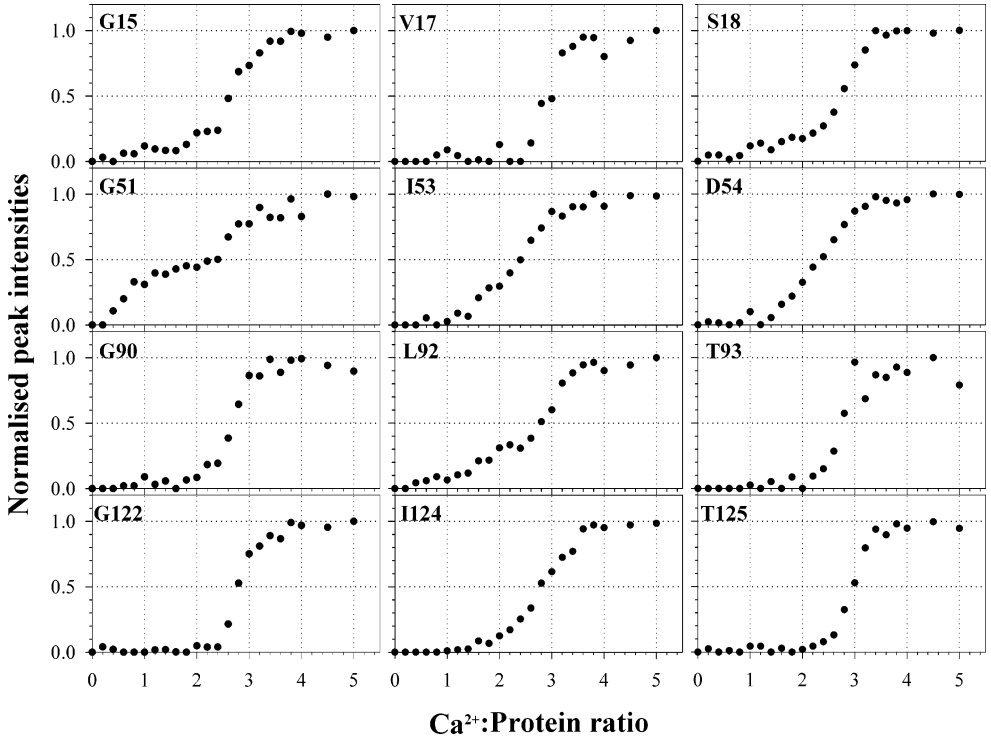


FIGURE 7: Plots of normalized peak volumes of the cross-peaks as a function of M/P ratio for residues at positions 6 (G15, G51, G90, and G122), 8 (V17, I53, L92, and I124), and 9 (S18, D54, T93, and T125) in all four metal binding sites of *Eh*CaBP. The amino acid residue is indicated at the top left of each individual panel.

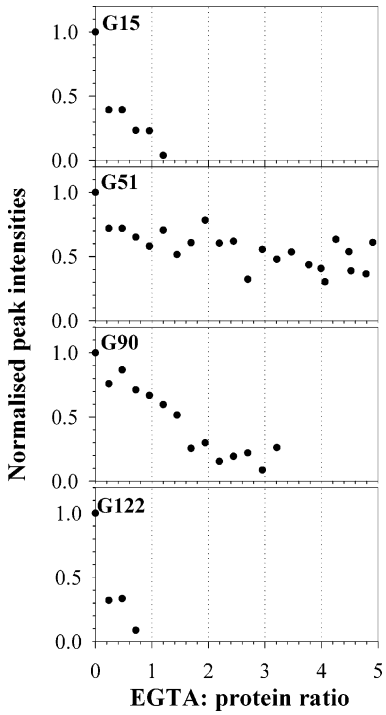


FIGURE 8: Plots of normalized peak volumes of G15, G51, G90, and G122 as a function of EGTA:protein ratio. The amino acid residue is indicated at the top left of each individual panel.

The hydrogen exchange of backbone amide protons in the apo state established the greater stability of the C-terminal domain compared to the N-terminal domain. The number of intact $^1H^N$ spins is found to be more in the C-terminal domain compared to the N-terminal domain. Further, the intact $^1H^N$ spins belong mostly to F-helices and $\beta$-strands of III and IV EF-hand units. Comparison of PFs for the apo and holo forms of *Eh*CaBP reveals that the PFs for apo are relatively very low compared to the same residues in the holo form. Within the apo form the C-terminal domain is found to be more structured than the N-terminal domain.

To ascertain which part of the tertiary structure is collapsed, we have used the information about the PFs estimated from the HX exchange data. The estimated PFs reveal that there is a substantial decrease in their protection when the protein transforms from the holo to apo form. We could estimate only seven PFs for the N-terminal domain, which reveals substantial collapse of its tertiary structure. This is supported by the nonobservance of the intact nature of the antiparallel $\beta$-strands in this domain, which brings the first two EF-hands (I and II) together.

Though we could estimate a relatively large number of PFs (22 in total) for the C-terminal domain, their absolute value is found to be substantially smaller compared to the corresponding values for the same residues in the holo form. This hints at the weakening of hydrogen bonds or/and hydrophobic interactions in this domain as well. As revealed by the HX experimental data, the third EF-hand in the C-terminal domain is found to be the most stable EF-hand. Interestingly, the number of amino acid residues belonging to the E-helix of the third EF-hand shows a considerable amount of protection. Incidentally, this helix is the longest among eight helices present in the holo form of the protein. Besides, residues at positions 2 (V86), 3 (D87), and 5 (D89) of the III $Ca^{2+}$ binding loop also show significant protection, which is not the case with the rest of the $Ca^{2+}$ binding loops present in the protein. Such protection may be due to the involvement of the respective backbone $^1H^N$ spins in hydrogen bonding. Earlier, it has been established that the $^1H^N$ of residues at positions 2 and 3 are involved in direct hydrogen bonding with the side-chain carboxylate oxygen of the most conserved Glu at position 12, while the $^1H^N$ of residue at position 5 is hydrogen bonded to the side-chain carboxylate oxygen of the residue at position 1 in the holo form (*2*). Similar hydrogen bonding may be retained in the III $Ca^{2+}$ binding loop of apo-*Eh*CaBP, thus making the III EF-hand structurally more ordered compared to the rest of the EF-hands.

The fact that all of the amino acid residues belonging to the two $\beta$-strands in the C-terminal domain show relatively high PFs reveal that the antiparallel $\beta$-sheet structure is intact even in the partially collapsed tertiary structure of the apo form of the protein. This is strongly supported by the large PFs seen for the backbone $^1H^N$ protons of 92 and 124, which remain intact even after 1000 s of the time interval in the HX experiment. Thus, within the C-terminal domain, well-protected $\beta$-strands may be able to communicate the binding of $Ca^{2+}$, leading to positive intradomain cooperativity between sites III and IV, which is not seen in the N-terminal domain. Closer examination of the $Ca^{2+}$ titration data (Figure 7) reveals that the $Ca^{2+}$ binding to site II does not trigger the binding of $Ca^{2+}$ to site I, while $Ca^{2+}$ binding to site III triggers binding of the metal to site IV. Such discrepancy in the intradomain cooperativity can be attributed to a better structured C-terminal domain.

*$Ca^{2+}$-Induced Protein Folding.* EF-hand proteins of the CaM superfamily are found to undergo major conformational change upon $Ca^{2+}$ binding (*2*, *3*, *9*−*12*). However, a variant of the EF-hand protein is found to lose a significant amount of tertiary structure in its apo form, which it regains after $Ca^{2+}$ binding. *Eh*CaBP belongs to such a variant (*13*−*17*). This property of collapsed secondary and tertiary structures helps us to understand its folding pathway, as monitored by $Ca^{2+}$ titration. As evident from Figure 7, $Ca^{2+}$ first binds to site II. During the initial stages of $Ca^{2+}$ titration, the $Ca^{2+}$ binding is slow and so is the protein folding (Figure 7). Until the M/P ratio of ~2.2 none of the other sites are occupied by $Ca^{2+}$. Beyond this concentration, sites I, III, and IV start folding almost together. On the other hand, EGTA titration shows that the removal of $Ca^{2+}$ is a sequential process wherein EGTA first chelates the bound $Ca^{2+}$ from site IV followed by sites I, III, and II, respectively. An important point to be noted is that, as depicted in both Figures 7 and 8, the well-conserved Gly in the sixth position of the EF-loop act as very good markers for $Ca^{2+}$ binding in EF-hand proteins.

*Both Apo- and Holo-EhCaBP Have Exposed Hydrophobic Surfaces.* ANS binding assay has been used earlier to monitor exposed hydrophobic moieties on the surface of calcium binding proteins and associated conformational changes during their folding (*34*). Calmodulin-like $Ca^{2+}$-sensor proteins undergo $Ca^{2+}$-induced conformational changes, exposing hydrophobic moieties to interact with target proteins. Hence, such proteins show negligible binding of ANS in their apo form, whereas they show strong binding to ANS in their holo form (*34*). In contrast, calbindin $D_{9K}$-like $Ca^{2+}$-buffer/transport proteins do not expose hydrophobic

moieties in either their apo or holo forms. Hence, they show negligibly small binding to ANS. In the present study, both holo- and apo-*Eh*CaBP show strong ANS binding, indicating that hydrophobic regions are exposed on the surface of *Eh*CaBP in both the apo and holo forms. Our earlier observations that the N-terminal domain of the apo-*Eh*CaBP has collapsed secondary and tertiary structures leading to the exposure of hydrophobic moieties could explain the enhanced fluorescence caused by ANS binding in the apo form.

*$Ca^{2+}$ Binding Affinities/Specifities Vis-à-Vis Lanthanides.* To characterize the factors that govern $Ln^{3+}$ binding to EF-hand proteins, we carried out earlier (*7*, *8*) $Yb^{3+}/Tm^{3+}$ substitution (paramagnetic probes) studies using NMR and calorimetry in holo-*Eh*CaBP. The titration experiments reveal that $Yb^{3+}/Tm^{3+}$ displaces $Ca^{2+}$ from the four metal binding sites in a sequential manner. $Yb^{3+}$ preferentially displaces $Ca^{2+}$ first from site III, and followed by sites II and I, and finally from site IV. It has been concluded that site III has the lowest affinity for $Ca^{2+}$, while site IV has the highest affinity. However, the present $Ca^{2+}$ titration of apo-*Eh*CaBP and EGTA titration of holo-*Eh*CaBP reveal that it is site II, which has the highest affinity for $Ca^{2+}$, while site IV has the lowest affinity. In light of these observations, the sequential $Ca^{2+}$ displacement by $Yb^{3+}/Tm^{3+}$ can only be attributed to $Ca^{2+}$ specificity of the corresponding EF-hand site, rather than $Ca^{2+}$ affinity.

Enthalpy titration curves of $Ca^{2+}$ studied earlier show the presence of four $Ca^{2+}$ binding sites in *Eh*CaBP, with two of them (low-affinity ones) in the N-terminal domain and the two other high-affinity sites in the C-terminal domain (*35*). The present NMR study reveals that the two higher affinity sites are sites II and III, one in the N-terminal and the other in the C-terminal domain, respectively. The above-mentioned studies taken together reveal that site IV has the lowest affinity and highest specificity for $Ca^{2+}$. It is site II which has the highest affinity among all four sites and higher specificity for $Ca^{2+}$ compared to sites I and III. Among the remaining sites, it is site III which has higher affinity compared to site I. The protein can be reversibly folded and unfolded upon addition of $Ca^{2+}$ and EGTA, respectively. Further, the $Ca^{2+}$ titration shows the gradual folding of the protein to its folded form from the molten globular apo state. As mentioned earlier, we have noticed that there are proteins of the calcium sensor family, such as neuronal calcium sensor-1 (*15*), which could have very weak tertiary structure in the apo form and a significantly ordered structure in the holo form (*13*−*17*). Such large conformational changes observed in transforming from the apo state to the holo state suggest that this protein should be functioning as a sensor protein and might have a significant role in host−parasite recognition.

## CONCLUSIONS

Apo-*Eh*CaBP essentially exists in a molten globular form with significantly collapsed secondary and tertiary structure. It regains its completely folded structure in the presence of $Ca^{2+}$. In the apo form, the C-terminal domain is more structured with the $\beta$-strands intact, compared to the N-terminal domain. This leads to positive intradomain cooperativity in the C-terminal domain. $Ca^{2+}$-induced folding shows a slow binding of $Ca^{2+}$ to site II, which then triggers binding of $Ca^{2+}$ to the remaining three metal binding sites. Thus, *Eh*CaBP belong to a variant of CaBPs, which undergoes considerable loss of tertiary structure on removal of $Ca^{2+}$. Such a variant of CaBP might play a vital role in signal transduction.

## ACKNOWLEDGMENT

The facilities provided by the National Facility for High Field NMR, supported by the Department of Science and Technology (DST), Department of Biotechnology (DBT), Council of Scientific and Industrial Research (CSIR), and Tata Institute of Fundamental Research, Mumbai, India, are gratefully acknowledged. We thank Prof. Alok Bhattacharya (JNU, New Delhi) for providing the *Eh*CaBP clone and Prof. Girjesh Govil and Dr. Yogendra Sharma (CCMB, Hyderabad) for critical comments.

## REFERENCES

1. Kretsinger, R. H., and Nockolds, C. E. (1973) Carp muscle calcium-binding protein. II. Structure determination and general description, *J. Biol. Chem. 248*, 3313−3326.
2. Strynadka, N. C., and James, M. N. (1989) Crystal structures of the helix-loop-helix calcium-binding proteins, *Annu. Rev. Biochem. 58*, 951−998.
3. Nelson, M. R., and Chazin, W. J. (1998) Structures of EF-hand Ca(2+)-binding proteins: diversity in the organization, packing and response to $Ca^{2+}$ binding, *Biometals 11*, 297−318.
4. Michael, J. B., Martin, D. B., and Peter, L. (1998) Calcium−a life and death signal, *Nature 395*, 645−648.
5. Atreya, H. S., Sahu, S. C., Bhattacharya, A., Chary, K. V. R., and Govil, G. (2001) NMR derived solution structure of an EF-hand calcium-binding protein from *Entamoeba histolytica*, *Biochemistry 40*, 14392−14403.
6. Allegrozzi, M., Bertini, I., Janik, M. B. L., Lee, Y. M., Liu, G., and Luchinat, C. (2000) Lanthanide induced pseudocontact shifts for solution structure refinements of macromolecules in shells up to 40 Å from the metal ion, *J. Am. Chem. Soc. 122*, 4154−4161.
7. Atreya, H. S., Mukherjee, S., Chary, K. V. R., Lee, Y. M., and Luchinat, C. (2003) Structural basis for sequential displacement of $Ca^{2+}$ by $Yb^{3+}$ in a protozoan EF-hand calcium binding protein, *Protein Sci. 12*, 412−425.
8. Mustafi, S. M., Mukherjee, S., Chary, K. V. R., Bianco, C. D., and Luchinat, C. (2004) Energetics and mechanism of Ca2+ displacement by lanthanides in a calcium binding protein, *Biochemistry 43*, 9320−9331.
9. Zhang, M., Tanaka, T., and Ikura, M. (1995) Calcium-induced conformational transition revealed by the solution structure of apo calmodulin, *Nat. Struct. Biol. 2*, 758−767.
10. Trave, G., Lacombe, P. J., Pfuhl, M., Saraste, M., and Pastore, A. (1995) Molecular mechanism of the calcium-induced conformational change in the spectrin EF-hands, *EMBO J. 14*, 4922−4931.
11. Houdusse, A., Love, M. L., Dominguez, R., Grabarek, Z., and Cohen, C. (1997) Structures of four $Ca^{2+}$-bound troponin C at 2.0 Å resolution: further insights into the $Ca^{2+}$-switch in the calmodulin superfamily, *Structure 5*, 1695−1711.
12. Wang, Z., Gergely, J., and Tao, T. (1992) Characterization of the Ca(2+)-triggered conformational transition in troponin C, *Proc. Natl. Acad. Sci. U.S.A. 89*, 11814−11817.
13. Lytle, B. L., Volkman, B. F., Westler, W. M., and Wu, J. H. (2000) Secondary structure and calcium-induced folding of the *Clostridium thermocellum* dockerin domain determined by NMR spectroscopy, *Arch. Biochem. Biophys. 379*, 237−244.
14. Precheur, B., Cox, J. A., Petrova, T., Mispelter, J., and Craescu, C. T. (1996) Nereis sarcoplasmic $Ca^{2+}$-binding protein has a highly unstructured apo state which is switched to the native state upon binding of the first $Ca^{2+}$ ion, *FEBS Lett. 395*, 89−94.
15. Jeromin, A., Muralidhar, D., Parameswaran, M. N., Roder, J., Fairwell, T., Scarlata, S., Dowal, L., Mustafi, S. M., Chary, K. V. R., and Sharma, Y. (2004) N-terminal myristoylation regulates calcium-induced conformational changes in neuronal calcium sensor-1, *J. Biol. Chem. 279*, 27158−27167.

16. Gombos, Z., Durussel, I., Ikura, M., Rose, D. R., Cox, J. A., and Chakrabartty, A. (2003) Conformational coupling of $Mg^{2+}$ and $Ca^{2+}$ on the three-state folding of calexcitin B, *Biochemistry 42*, 5531−5539.
17. Yamniuk, A. P., Nguyen, L. T., Hoang, T. T., and Vogel, H. J. (2004) Metal ion binding properties and conformational states of calcium- and integrin-binding protein, *Biochemistry 43*, 2558−2568.
18. Kuboniwa, H., Tjandra, N., Grzesiek, S., Ren, H., Klee, C. B., and Bax, A. (1995) Solution structure of calcium-free calmodulin, *Nat. Struct. Biol. 2*, 768−776.
19. Gagne, S. M., Tsuda, S., Li, M. X., Smillie, L. B., and Sykes, B. D. (1995) Structures of the troponin C regulatory domains in the apo and calcium-saturated states, *Nat. Struct. Biol. 2*, 784−789.
20. Tanaka, T., Ames, J. B., Harvey, T. S., Stryer, L., and Ikura, M. (1995) Sequestration of the membrane-targeting myristoyl group of recoverin in the calcium-free state, *Nature 376*, 444−447.
21. Loftus, B., Anderson, I., Davies, R., Alsmark, U. C., Samuelson, J., Amedeo, P., Roncaglia, P., Berriman, M., Hirt, R. P., Mann, B. J., Nozaki, T., Suh, B., Pop, M., Duchene, M., Ackers, J., Tannich, E., Leippe, M., Hofer, M., Bruchhaus, I., Willhoeft, U., Bhattacharya, A., Chillingworth, T., Churcher, C., Hance, Z., Harris, B., Harris, D., Jagels, K., Moule, S., Mungall, K., Ormond, D., Squares, R., Whitehead, S., Quail, M. A., Rabbinowitsch, E., Norbertczak, H., Price, C., Wang, Z., Guillen, N., Gilchrist, C., Stroup, S. E., Bhattacharya, S., Lohia, A., Foster, P. G., Sicheritz-Ponten, T., Weber, C., Singh, U., Mukherjee, C., El-Sayed, N. M., Petri, W. A., Jr., Clark, C. G., Embley, T. M., Barrell, B., Fraser, C. M., and Hall, N. (2005) The genome of the protist parasite *Entamoeba histolytica*, *Nature 433*, 865−868.
22. Makioka, A., Kumagai, M., Kobayashi, S., and Takeuchi, T. (2002) Possible role of calcium ions, calcium channels and calmodulin in excystation and metacystic development of *Entamoeba invadens*, *Parasitol. Res. 88*, 837−843.
23. Sahu, S. C., Bhattacharya, A., Chary, K. V. R., and Govil, G. (1999) Secondary structure of a calcium binding protein (CaBP) from *Entamoeba histolytica*, *FEBS Lett. 459*, 51−56.
24. Kay, L. E., Keifer, P., and Saarinen, T. (1992) Pure absorption gradient enhanced heteronuclear single quantum correlation spectroscopy with improved sensitivity, *J. Am. Chem. Soc. 114*, 10663−10665.
25. Bai, Y., Milne, J. S., Mayne, L., and Englander, S. W. (1993) Primary structure effects on peptide group hydrogen exchange, *Proteins 17*, 75−86.
26. Linse, S., and Chazin, W. J. (1995) Quantitative measurements of the cooperativity in an EF-hand protein with sequential calcium binding, *Protein Sci. 4*, 1038−1044.
27. Rao, B. D. N. (1989) Nuclear magnetic resonance line-shape analysis and determination of exchange rates, *Methods Enzymol. 176*, 279−311.
28. Baum, J., Dobson, C. M., Evans, P. A., and Hanley, C. (1989) Characterization of a partly folded protein by NMR methods: studies on the molten globule state of guinea pig alpha-lactalbumin, *Biochemistry 28*, 7−13.
29. Schulman, B. A., Kim, P. S. Dobson, C. M., and Redfield, C. (1997) A residue-specific NMR view of the non-cooperative unfolding of a molten globule, *Nat. Struct. Biol. 4*, 630−634.
30. Kobayashi, T., Ikeguchi, M., and Sugai, S. (2000) Molten globule structure of equine beta-lactoglobulin probed by hydrogen exchange, *J. Mol. Biol. 299*, 757−770.
31. Halskau, O., Froystein, N. A., Muga, A., and Martinez, A. (2002) The membrane-bound conformation of alpha-lactalbumin studied by NMR-monitored $^1H$ exchange, *J. Mol. Biol. 321*, 99−110.
32. Falke, J. J., Drake, S. K., Hazard, A. L., and Peersen, O. B. (1994) Molecular tuning of ion binding to calcium signaling proteins, *Q. Rev. Biophys. 27*, 219−290.
33. Biekofsky, R. R., Martin, S. R., Browne J. P., Bayley, P. M., and Feeney, J. (1998) $Ca^{2+}$ coordination to backbone carbonyl oxygen atoms in calmodulin and other EF-hand proteins: $^{15}N$ chemical shifts as probes for monitoring individual-site $Ca^{2+}$ coordination, *Biochemistry 37*, 7617−7629.
34. Berggard, T., Silow, M., Thulin, E., and Linse, S. (2000) $Ca^{2+}$ and $H^+$ dependent conformational changes of calbindin D28k, *Biochemistry 39*, 6864−6873.
35. Gopal, B., Swaminathan, C. P., Bhattacharya, S., Bhattacharya, A., Murthy, M. R., and Surolia, A. (1997) Thermodynamics of metal ion binding and denaturation of a calcium binding protein from *Entamoeba histolytica*, *Biochemistry 36*, 10910−10916.

BI050691H